Time-Aware Robot Motion Planning for Non-Planar 3D Concrete Printing

Yuxin Lin[1][0000-0002-3867-820X], Mania Aghaei Meibodi[1][0000-0003-2867-6814], and Kira Barton[2][0000-0003-1047-8078]

[1] University of Michigan, Taubman College of Architecture and Urban Planning, Ann Arbor, MI, USA
[2] University of Michigan, Robotics Department, Ann Arbor, MI, USA
linyuxin@umich.edu

Abstract. Non-planar 3D concrete printing (3DCP) improves geometric fidelity for complex optimized structures, but it tightly couples volumetric feedforward velocity with rapid printhead reorientation. With constant pump rate, the required filament geometry sets the feedforward velocity and a fixed traversal time per segment; however, the orientation changes demanded within this time can exceed robot kinematic limits, causing slowdowns and over-extrusion. We present a motion planning framework that addresses this conflict by coupling a volumetric feedforward velocity model with a global SO(3) optimization on printing orientation. The method is simulated in KUKA|prc and is executed on a 6-DoF KUKA robot printing a topology-optimized branched beam. Simulation and preliminary printing results show reduced robot angular-velocity peaks and smoother joint motion, while maintaining commanded feedforward velocities for accurate filament dimensions.

Keywords: Feedforward Variable Velocity · Orientation optimization · Variable Printing Directions · Data-driven approach

1 Introduction

Materially optimized concrete structures (MOCS) often exhibit non-coplanar interfaces, high-genus surfaces, and overhangs that are difficult to fabricate with planar slicing [1]. Planar slicing introduces staircase effects and reduce geometric fidelity in inclined or curved regions. Non-planar slicing mitigates these issues by generating contours that follow the target geometry, thereby preserving geometric accuracy and reducing the staircase effect [2,3].

The execution of non-planar 3D concrete printing (3DCP) must satisfy two linked requirements in Fig. 1a: (i) maintain consistent filament width under variable layer height by regulating the deposition rate via the robot linear velocity at a constant pump rate [4], and (ii) continuously reorient the printhead to follow slice-informed, surface-aligned printing directions [5,6].

These two requirements create a time-feasibility conflict in Fig. 1b: the volumetric requirements derive the linear velocity for each segment, but the robot

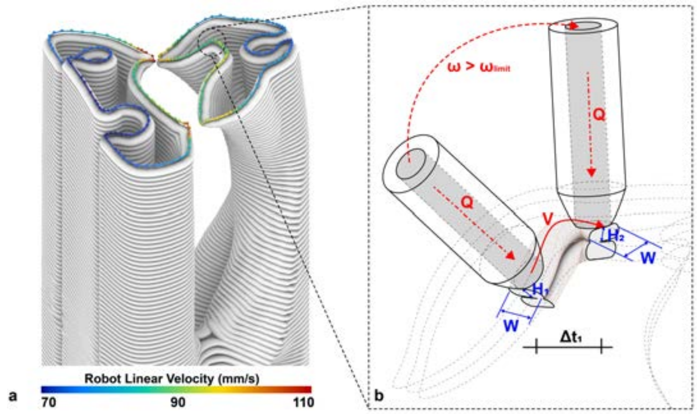

Fig. 1. (a) Two coupled requirements for non-planar 3DCP: Variable robot velocity for volumetric deposition and surface-aligned printing directions. (b) Conflict: the constant pump flow Q, width W and heights H_1, H_2 set a velocity V and traversal time Δt_1. The required rotation between two endpoints over Δt_1 can demand an angular velocity ω. If ω exceeds the limit ω_{limit}, the motion is kinematically infeasible.

may require more time to realize the corresponding orientation changes within joint limits. The robot then slows down, causing over-extrusion. Alternatively, limiting orientation change to preserve velocity sacrifices surface alignment and re-introduce staircase effects. Therefore, non-planar 3DCP requires motion planning that jointly preserves volumetric deposition and ensures time-aware orientation change within required time windows.

2 Literature Review

Existing non-planar motion planning strategies for 3D printing (3DP) can be broadly grouped into two categories: (i) methods that focus on orientation feasibility and collision avoidance (e.g. selecting robot configurations within orientation cones around surface-aligned printing directions) [7], and (ii) methods that couple non-planar printpath with process parameters by regulating robot velocity, extrusion flow rate, and printhead orientation to preserve filament dimensions and surface quality [8,9].

Beyond 3DP, robot trajectory planning for complex geometries tasks (e.g. spraying/coating) jointly optimizes paths and orientations to achieve smooth, time-aware motions [10,11]; however, these strategies typically allow the path to be freely altered as long as coverage and smoothness are satisfied. Therefore, they cannot be directly applied to 3DCP, where the printpath is fixed by slicing.

To the best of our knowledge, no prior work jointly accounts for time-feasible orientation changes and the slice-informed, volumetric feedforward linear velocity required along a non-planar printpath in 3DCP. This gap is particularly critical in 3DCP, where large nozzles, thick filaments, and fresh-state material behavior make the process highly sensitive to deposition errors. Motivated by this, we propose a method that ensures kinematic feasibility while preserving volumetric deposition requirements.

3 Method: Volumetric Feedforward Velocity and Time-Aware Orientation Optimization

We propose a two-stage motion planning framework that couples volumetric deposition with time-feasible reorientation. Stage 1 computes a segment-wise feedforward linear velocity from a volumetric model at constant pump flow, which also defines the segment traversal time. Stage 2 performs a global SO(3) optimization to refine printhead orientations so that required reorientations are feasible within these time windows while staying close to the slice-informed directions that mitigate staircase effects.

3.1 Stage 1: Feedforward Velocity via Volumetric Calculation

Assuming constant volumetric flow rate Q, the velocity V is given by Eq. (1):

$$V = \frac{Q}{\bar{A}}, \qquad \bar{A} = w_E \frac{h_1 + h_2}{2} + k \frac{h_1^2 + h_1 h_2 + h_2^2}{3}, \qquad k = \frac{\pi - 4}{4}. \tag{1}$$

Here $\bar{A}$ is the segment-averaged filament cross-sectional area under a capsule approximation with constant filament width w_E and projected layer heights h_1 and h_2 at the segment endpoints (Fig. 2). We assume that the projected height varies linearly within each short segment, thus deriving $\bar{A}$ used above. For segment length ΔL, the traversal time is given by Eq. (2):

$$\Delta t = \frac{\Delta L}{V}, \tag{2}$$

which is treated as the time window for the orientation change between consecutive poses.

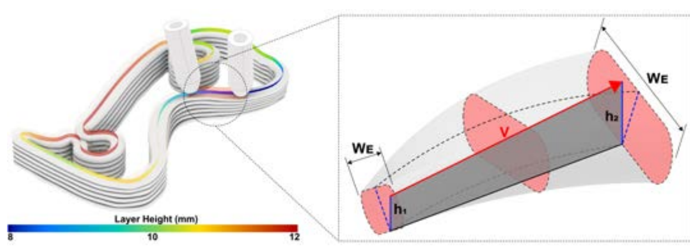

Fig. 2. Non-planar printpaths in the left image feature variable layer heights; to maintain a uniform filament width, a volumetric model for feedforward velocity calculation is required. The highlighted segment in the right image is modeled as a capsule-shaped filament with constant width w_E and projected layer heights h_1 and h_2 at its two ends; together with the segment length, these parameters define the average effective cross-sectional area used to compute the feedforward velocity.

3.2 Stage 2: Global SO(3) Optimization for Time-Aware Orientation Regulation

To ensure time-feasible reorientation under the segment-wise time window from Stage 1 while remaining close to the slice-informed printing direction, we model the printhead orientation at sample i as $R_i \in \mathrm{SO}(3)$. For each segment, we compute the relative rotation $\delta\boldsymbol{\phi}_i = \mathrm{Log}(R_i^\top R_{i+1})^\vee$ and the corresponding required angular velocity $\omega_i^{\mathrm{req}} = \|\delta\boldsymbol{\phi}_i\|/\Delta t$. These quantities are then used to regulate orientation updates in the global SO(3) optimization.

Energy function. We solve for $\{R_i\}$ by minimizing a least-squares objective that balances geometric fidelity, smoothness, and time-dependent kinematic feasibility using Eq. (3).

$$E_{\mathrm{orientation}}(\{R_i\}) = \underbrace{\sum_i \|\log(R_i^\top \hat{R}_i)\|^2}_{\textbf{Geometric fidelity}} + \lambda \underbrace{\sum_i \|\log(R_i^\top R_{i+1})\|^2}_{\textbf{Smoothness}} + \gamma \underbrace{\sum_i \left[\omega_i^{\mathrm{req}} - \omega_{\max}\right]_+^2}_{\textbf{Kinematic limit}} + \kappa \underbrace{\sum_i (\Delta\psi_i)^2}_{\textbf{Yaw consistency}} . \quad (3)$$

Interpretation. $\hat{R}_i$ is the original slice-defined, surface-aligned orientation and $\Delta\psi_i$ is the yaw rotation around the extrusion axis. In Eq. (3), the terms enforce (i) *geometric fidelity* to $\hat{R}_i$, (ii) *smoothness* by penalizing sharp rotations which can cause excessive vibration, (iii) *kinematic feasibility* via a hard penalty active only when $\omega_i^{\mathrm{req}} > \omega_{\max}$, and (iv) *yaw consistency* to limit twist about the extrusion axis and reduce hose/cable torsion. Squared norms are used to obtain the least-squares objective in which larger deviations are penalized more strongly

Weights selection and optimization. The geometric fidelity term sets the reference scale; λ, γ, and κ are tuned empirically to trade off smoothness, kinematic feasibility, and yaw consistency. Minimization is performed on SO(3) via Gauss-Newton, updating each orientation with the exponential map in Eq. (4):

$$R_i \leftarrow R_i \exp([\delta\boldsymbol{\phi}_i]_\times). \quad (4)$$

4 Experimental Studies through Simulation and Physical Printing

Setup. To validate the proposed motion planning framework, we conducted experimental studies that combine simulation-based analysis and physical printing tests. A printing simulation is performed in KUKA|prc to preview the resulting robot poses and printhead orientations before physical execution. Physical printing is performed on a 6-DoF KUKA industrial robot equipped with a MAI multi-mixing pump delivering material at a constant flow rate. The topology-optimized branched beam prototype shown in Fig. 3 is used as the test geometry, with particular focus on the highly non-planar areas at bottom and the overhanging branched regions.

Datasets. Two dataset categories are collected to evaluate both robot execution and the resulting printed geometry.

- *Robot motion data* include computed feedforward velocities, simulated orientation and angular-velocity profiles, simulated joint trajectories, and real-time robot motion logs recorded during printing.
- *Construction data* include layer-width measurements and visual inspection of the as-printed geometry.

Benchmarking and Validation. The evaluation compares robot motion data from the proposed method against a baseline derived directly from the non-planar slicing output. The *baseline* uses slicing-informed orientations with a feedforward velocity profile, without regulating orientation changes. The *optimized case* refines orientations via SO(3) and then recomputes the feedforward velocity profile from the updated orientations to maintain volumetric deposition accuracy.

Fig. 3. Experimental validation of the proposed motion-planning framework on a topology-optimized branched beam. The complex geometric features make it a representative case for studying the coupled requirements of time-dependent orientation feasibility and volumetric accuracy.

5 Results

Simulation and physical printing use a constant pump rate of $Q = 1.4\,\mathrm{L/min}$ and a nominal layer width of 30 mm, which together define the segment-wise feedforward velocity and traversal time. The simulation results first validate the effect of the global SO(3) optimization under these volumetric requirements. Physical experiments then assess whether these improvements carry over to actual non-planar 3D concrete printing.

5.1 Robot Motion Data Validation

Simulation. The simulation results highlight that the energy function E decreases significantly after optimization, indicating that the method finds an orientation sequence that better balances surface alignment and respects the smooth and time-feasible rotation of the printhead. As shown in Fig. 4a, the optimized orientation sequence contains fewer abrupt jumps and exhibits significantly lower reorientation per segment. As a result, this optimization directly reduces the required printhead angular velocity: segments that originally demanded rapid and near-limit rotations become more gradual, reducing angular velocity peaks that would otherwise exceed the robot's allowable rotational rate within the fixed time window.

To further validate the effect of optimization on the feasibility of the robot pose, the angle of the joints before and after regulation was analyzed for all six axes in Fig. 4b. The original joint angles over time for the A1-A6 axes show unfeasible angles and sharper changes, while the optimized one shows the joint motions are smoother and more stable, indicating more feasible and coordinated robot poses.

Real-Time Robot Motion Data. After orientation regulation, the segment-wise velocity profile was recomputed, shown in Fig. 4c, for new printing directions with their corresponding volumetric requirements. Real-time robot motion data was collected and mapped back onto the non-planar filament and visualized in Fig. 5. The robot closely operated at the commanded feedforward velocity while maintaining the desired printhead orientation, without noticeable slow-down events in the highly curved non-planar regions. The deviation between commanded and measured velocities remains within approximately 5% throughout the printing process.

5.2 Construct Data Results

The printed part was examined during printing and after curing through visual inspection and manual measurements at critical areas in Fig. 6, including the extreme non-planar base, overhanging areas, and branching areas. Across these locations, caliper measurements of layer height and layer width closely matched the design, with most layers remaining well aligned with the non-planar printpath and maintaining intended dimensions of around 30 mm without over-extrusion.

However, further inspection in Fig. 6 showed the appearance of deformation, which was non-uniform throughout the construct and was more noticeable in regions with large printhead tilts. Our assumption is that the printhead rotational motion affects fresh material behavior and should be systematically investigated in future work.

6 Discussion

During fabrication of the topology-optimized branched beam segment, the feed-forward velocity profile derived from volumetric calculation reliably preserved

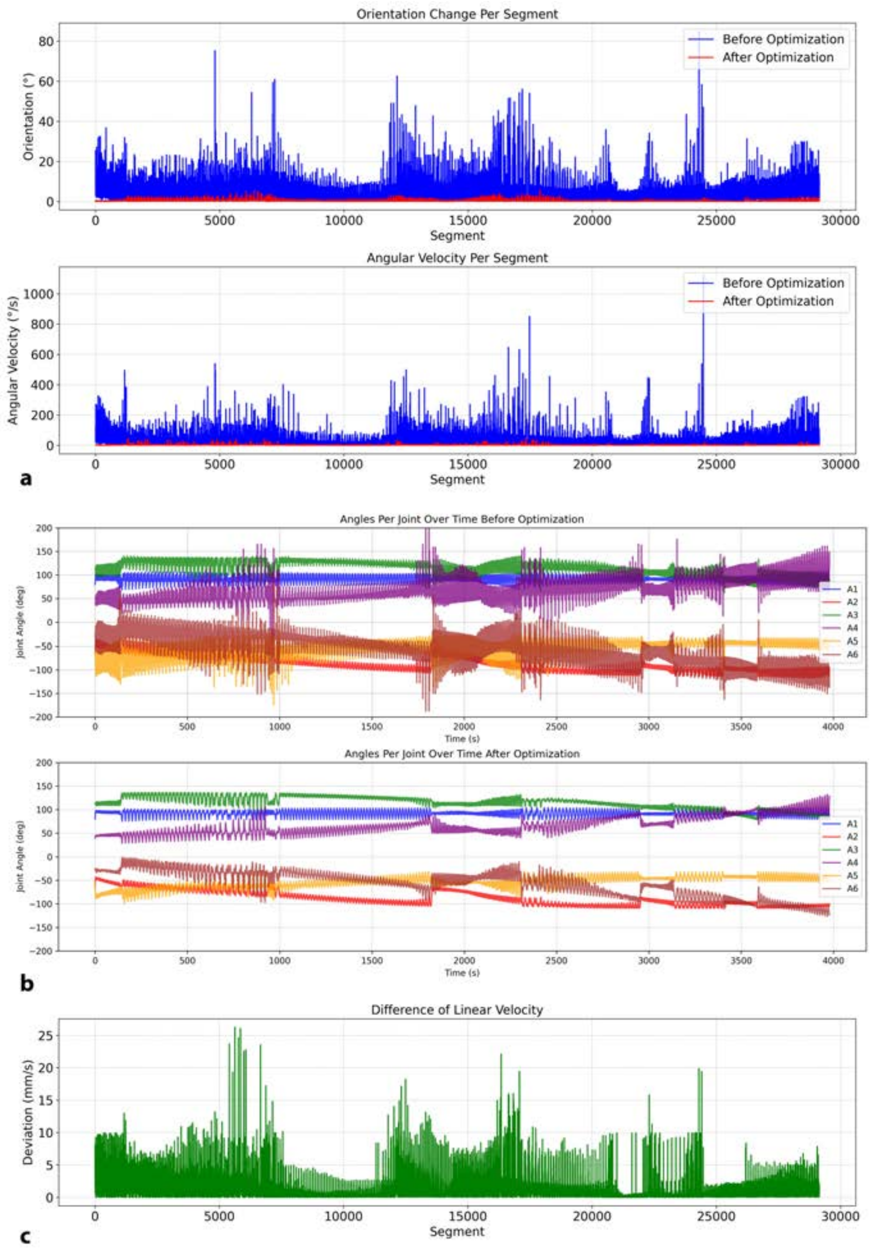

Fig. 4. (a): Comparison of segment-wise orientation change (top) and angular velocity (bottom) of the printhead before and after global SO(3) optimization. (b): Joint angles over time for all six robot axes before (top) and after (bottom) orientation optimization, showing smoother and more feasible joint motions after optimization. (C): The difference of robot linear velocity before and after optimization.

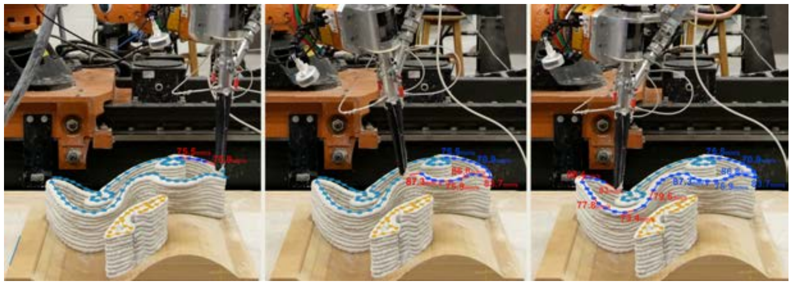

Fig. 5. Real-time collected robot motion data has been mapped onto the printed non-planar filament.

Fig. 6. View of the printed optimized beam segment showing consistent layer height and width across multiple areas, along with noticeable deformation in certain regions.

the intended layer width across regions with varying layer heights, confirming that the feedforward velocity successfully remained effective due to the orientation optimization. In the critical areas within the optimized beam-including the extreme non-planar areas and overhanging branched regions—where abrupt orientation changes often occur, the proposed robot motion planning framework reduced angular-velocity peaks and eliminated slowdown events that would otherwise induce over-extrusion. Measurements on the printed construct showed layer width deviations below 2 mm, along with improved overall geometric accuracy. Together, these experiments indicate that integrating feedforward velocity with time-aware SO(3) orientation optimization yields robust and physically feasible motion plans for complex, non-planar 3DCP.

Future work will extend the framework by incorporating joint-acceleration ramp into the motion planning and systematically examining how different acceleration profiles influence deposition performance and surface finish. Also, we will investigate how coupled variations in printhead orientation and angular velocity affect fresh-state material behavior (particularly deformation) during deposition, and how these effects propagate from local filament to the overall construct.

Acknowledgements This research was funded by University of Michigan's Michigan Materials Research Institute (MMRI) to Dr. Mania Aghaei Meibodi and Dr. Kira Barton, and the National Science Foundation CAREER Award [NSF CAREER-2441176 CMMI] to Dr. Mania Aghaei Meibodi.

References

1. Meibodi, M.A., Kamhawi, A., Dehnavi, A.F., Li, Y.: Non-planar slicing for high-genus surfaces with non-coplanar interfaces. Virtual and Physical Prototyping **21**(1), e2603853 (2026). https://doi.org/10.1080/17452759.2025.2603853, https://doi.org/10.1080/17452759.2025.2603853
2. Lin, Y., Bayramvand, A., Aghaei Meibodi, M.: Towards lightweight structure: Coupling topology optimization with non-planar 3D concrete printing. In: Computational Design and Robotic Fabrication, pp. 3–12. Springer Nature Singapore, Singapore (2025)
3. Meibodi, M.A., Lin, Y., Chen, H.: Hybrid approaches towards 3D concrete printing for lightweight reinforced concrete structures. Digital Concrete 2024 (2024). https://doi.org/https://doi.org/10.24355/dbbs.084-202408140649-0
4. Anton, A., Reiter, L., Wangler, T., Frangez, V., Flatt, R.J., Dillenburger, B.: A 3D concrete printing prefabrication platform for bespoke columns. Autom. Constr. **122**(103467), 103467 (2021)
5. Zhi, Y., Chai, H., Teng, T., Akbarzadeh, M.: Automated toolpath design of 3D concrete printing structural components. Addit. Manuf. **100**(104662), 104662 (2025)
6. Lowke, D., Anton, A., Buswell, R., Jenny, S.E., Flatt, R.J., Fritschi, E.L., Hack, N., Mai, I., Popescu, M., Kloft, H.: Digital fabrication with concrete beyond horizontal planar layers. Cement and Concrete Research **186**, 107663 (2024). https://doi.org/https://doi.org/10.1016/j.cemconres.2024.107663
7. Mitropoulou, I., Bernhard, M., Dillenburger, B.: Print paths key-framing: Design for non-planar layered robotic FDM printing. In: Symposium on Computational Fabrication. ACM, New York, NY, USA (2020)
8. Shembekar, A.V., Yoon, Y.J., Kanyuck, A., Gupta, S.K.: Trajectory planning for conformal 3D printing using non-planar layers. In: Volume 1A: 38th Computers and Information in Engineering Conference. American Society of Mechanical Engineers (2018)
9. Llewellyn-Jones, T., Allen, R., Trask, R.: Curved layer fused filament fabrication using automated toolpath generation. 3D Print. Addit. Manuf. **3**(4), 236–243 (2016)
10. Pelzer, L., Hopmann, C.: Additive manufacturing of non-planar layers with variable layer height. Addit. Manuf. **37**(101697), 101697 (2021)
11. Grassmann, R., Johannsmeier, L., Haddadin, S.: Smooth point-to-point trajectory planning in se (3)with self-collision and joint constraints avoidance. In: 2018 IEEE/RSJ International Conference on Intelligent Robots and Systems (IROS). pp. 1–9 (2018). https://doi.org/10.1109/IROS.2018.8594339